

# Ultra-Low-Field MRI and Spin-Lattice Relaxation Time of $^1\text{H}$ in the Presence of $\text{Fe}_3\text{O}_4$ Magnetic Nano-Particles Detected With a High- $T_C$ DC-SQUID

Ning Wang, Yirong Jin, Fengying Jiang, Jianfeng Zeng, Mingyuan Gao, Yulin Wu, Hui Deng, Guolin Zheng, Jie Li, Yingfei Chen, Ye Tian, Yufeng Ren, Genghua Chen, and Dongning Zheng

**Abstract**—We have carried out ultra-low-field nuclear magnetic resonance (NMR) and magnetic resonance imaging experiments in microtesla magnetic fields using a high- $T_C$  dc-SQUID sensor. The measurements were carried out in a home-made magnetically shielded room. NMR spectra of  $^1\text{H}$  from tap water and other substance samples were obtained in the field range from 10–200  $\mu\text{T}$ . By adapting a transformer coupled detection system, the signal-to-noise ratio of NMR peak in a single-shot measurement for 10 ml tap water was increased significantly as compared with our previously used direct detection method. The improvement was attributed to the increased coupling efficiency and reduced SQUID noise. By applying magnetic field gradient in three directions, one- and two-dimensional imaging results were obtained from water phantom samples. Furthermore, the effect of  $\text{Fe}_3\text{O}_4$  magnetic nanoparticles on the spin-lattice relaxation time  $T_1$  was studied.

**Index Terms**—Magnetic resonance imaging, nuclear magnetic resonance, superconducting quantum interference device (SQUID).

## I. INTRODUCTION

**N**UCLEAR MAGNETIC resonance (NMR) and magnetic resonance imaging (MRI) are powerful tools widely used in scientific and industrial research, and clinic diagnoses. In the conventional induction detection method, the signal detected by the pick-up coil is proportional to the square of magnetic field. Therefore, great effort has been made to develop NMR systems operating at higher and higher magnetic fields. However, NMR and MRI working with very low magnetic fields has constantly attracted substantial attention and been explored

Manuscript received October 10, 2012; accepted December 23, 2012. Date of publication January 9, 2013; date of current version February 6, 2013. This work was supported in part by the Ministry of Science and Technology of China under Grant 2011CBA00106 and Grant 2009CB929102, and by the National Science Foundation of China under Grant 11104333, Grant 10974243, and Grant 11161130519.

N. Wang and G. Zheng are with the Institute of Physics and National Laboratory for Condensed Matter Physics, Chinese Academy of Sciences, Beijing 100190, China. They are also with the 16th Institute of China Electronics Technology Group Corporation, Hefei 230043, China.

Y. Jin, Y. Wu, H. Deng, J. Li, Y. Chen, Y. Tian, Y. Ren, G. Chen, and D. Zheng are with the Institute of Physics and National Laboratory for Condensed Matter Physics, Chinese Academy of Sciences, Beijing 100190, China (e-mail: dzheng@aphy.iphy.ac.cn).

F. Jiang is with the Institute of Physics and National Laboratory for Condensed Matter Physics, Chinese Academy of Sciences, Beijing 100190, China. She is also with the School of Science, Beijing University of Posts and Telecommunications, Beijing 100876, China.

J. Zeng and M. Gao are with the Institute of Chemistry, Beijing 100190, China.

Color versions of one or more of the figures in this paper are available online at <http://ieeexplore.ieee.org>.

Digital Object Identifier 10.1109/TASC.2013.2238573

for various kinds of reasons [1]. Because of the rapid decrease of the signal sensitivity with decreasing magnetic field for conventional induction coil sensors, a number of alternative sensors have been investigated to record NMR signal at very low fields [2]. In recent years, ultra-low field (ULF, typically in the microtesla range) NMR and MRI using superconducting quantum interference device (SQUID) as signal detectors has received much attention to explore a variety of new applications [3]–[16]. It is believed that the ULF-NMR/MRI could be a useful and prospective supplement to high-field systems because the ultra-low field means the significant simplification in coil design and construction that could lead to possibly simple, inexpensive and portable NMR or MRI systems. At present, both low- $T_C$  and high- $T_C$  SQUID devices have been used in ULF-NMR/MRI. The advantages of low- $T_C$  SQUID devices include the reliability, high sensitivity, and availability of wired gradiometer coils that ensure the SQUID performance not be compromised by the magnetic fields applied in the measurements. In contrast, for high- $T_C$  SQUIDs, the sensitivity is lower and there is no superconducting wire gradiometers at present. However, the cryogenic system is easy to operate and maintain for high- $T_C$  SQUID, this is a big advantage and makes high- $T_C$  SQUID attractive in many circumstances.

Here we report our experimental study on ULF-NMR and MRI based on a high- $T_C$  dc-SQUID sensor. At first, we present a detailed description about the experimental setup. Then, we show the results of one-dimensional and two-dimensional MRI results. Finally, we investigate the effect of  $\text{Fe}_3\text{O}_4$  magnetic nano-particles on the spin-lattice relaxation time  $T_1$  and two-dimensional (2D) dimensional MRI.

## II. EXPERIMENTAL

The measurements were performed in a home-made simple magnetically shielded room (MSR) which consists of a 2 mm thick  $\mu$ -metal layer, a 4 mm thick cooper layer and a 10 mm thick soft iron layer [1]. The shielding factor is about 12 at 0.01 Hz, and above 2000 at frequency higher than 100 Hz. The inner dimension of the MSR is  $2.4 \times 2.4 \times 2.4 \text{ m}^3$ . The residual field around the center of the MSR is about 100 nT in the vertical direction whereas the slow variation of the residual field is generally less than 1 nT in the night and could be as large as a few nano-tesla during the day time.

Experiments were initially performed using a direct coupled scheme [16] in which the SQUID sensor was placed in a

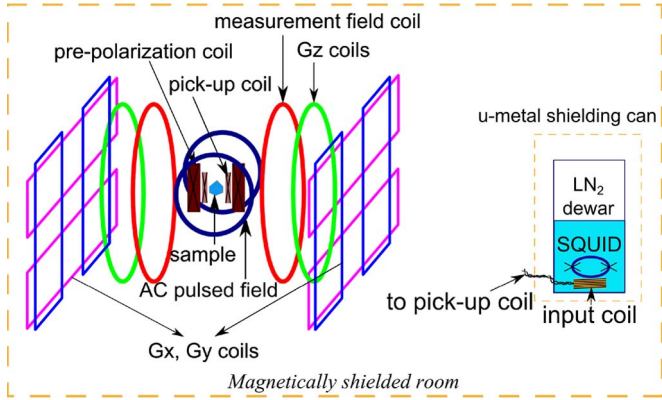


Fig. 1. Schematic of the measurement system.

liquid nitrogen dewar. Under this arrangement, the SQUID sensor was exposed to the strong pre-polarization field that caused flux trapping in the pickup-loop of the SQUID sensor and the SQUID noise performance was degraded significantly even though the SQUID active plane was carefully adjusted to make it as parallel to the applied field as possible. In order to improve the signal to noise ratio (SNR) of the experiment, we adapted a scheme in which the free-induction-decay (FID) from resonance was detected by a copper coil wound around the sample and then transferred to an input coil closely beneath the SQUID sensor through twisted copper wire pair, similar to that reported in ref [12]. In this transformer arrangement, the SQUID sensor and the input coil were placed inside a 3-layer  $\mu$ -metal shielded liquid nitrogen dewar and a capacitance was added in the loop to form a LC circuit, which enhanced the signal at the resonance frequency. The pre-polarization coil was a large solenoid wound surrounding the pickup coil. The measurement field  $B_0$  was supplied by a pair of Helmholtz coils of 0.6 m diameter. A pair of Maxwell coils of 0.6 m diameter was used to generate the gradient field along the measurement field ( $G_z$ ). Two sets of biplane coil pair were also added to generate the gradient field on the two other directions ( $G_x$  and  $G_y$ ). To reduce the interference to the SQUID during the pre-polarization and measurement, relays were used in the detection loop and in the pre-polarization loop. We found that by connecting a resistor in parallel to the detection coil could significantly reduce the disturbance to the SQUID when the relays were switched off and on. We call this system coil transformer coupled detection system. It is schematically shown in Fig. 1. The gradient fields produced by  $G_y$  and  $G_z$  coils were measured by a fluxgate magnetometer. The data are shown in Fig. 2.

The pre-polarization field was about 16 mT and the measurement field was between 10 to 110  $\mu\text{T}$ . For a 10 ml tap water sample, we found that the SNR was increased to 30 from 4 measured in the direct detection method. The improvement of the SNR can be mainly attributed to the improvement of the coupling efficiency and the reduction of the SQUID noise level. It is expected that by further increasing the magnitude of  $B_p$ , the SNR value can be further increased as demonstrated by others [4], [8], [12]. We have constructed a water cooled copper coil that expected to increase  $B_p$  to about 60 mT. Preliminary results showed that the signal could indeed be increased.

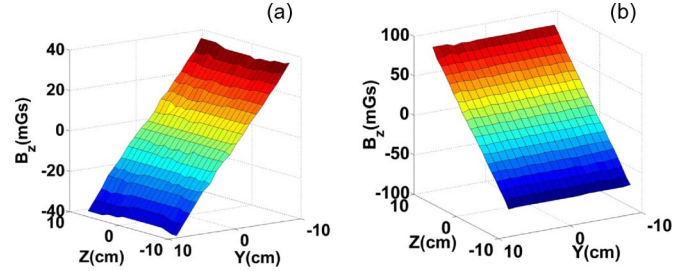


Fig. 2. Measured results of  $z$ -component (along  $B_0$ ) distribution in  $yz$ -plane. (a)  $B_z$  generated by  $G_y$  coils (biplane coils), the current was 1.1 A. The gradient of  $G_y$  was estimated to 359 nT/cm  $\cdot$  A. (b)  $B_z$  generated by  $G_z$  coils (Maxwell coils), the current was 0.5 A. The gradient of  $G_z$  was estimated to 1570 nT/cm  $\cdot$  A.

Although the coil transformer (includes the pick-up coil, input coil and the connection wires) itself introduced additional Johnson noise, we could control it to a level less than or comparable with the noise of the SQUID sensor. Moreover, we have conducted measurements by using the coupled detection method with the SQUID sensor and with a room temperature amplifier (SR560) on the present coil setup. The comparison of the results showed that the measurement with SQUID sensor provide a higher SNR than the measurement with the room temperature amplifier in the frequency range 1–7 kHz. Thus, using the high- $T_C$  SQUID can reduce the measurement time and increase the resolution.

For magnetic resonance imaging measurements, magnetic field gradients were applied. It was found that the residual field gradient inside the MSR could distort the NMR peak. Sometimes, the peak could be split. To reduce this effect, we apply field gradients  $G_x$ ,  $G_y$ , and  $G_z$  prior the measurements. During the MRI experiments further field gradients of  $G_y$  and  $G_z$  were applied. The two-dimensional MRI was taken using the back projection method with the gradient field rotated  $15^\circ$  for each imaging sequence. The pre-polarization time was about 8 s in most case. The pre-polarization field  $B_p$  was switched off in less than 1 ms and no  $\pi/2$  pulse was used. The spin-echo signal was recorded for imaging.

To study the effect of magnetic nano-particles on the spectra and images, we choose  $\text{Fe}_3\text{O}_4$  nano-particles. The average size of the  $\text{Fe}_3\text{O}_4$  MNP in the fluid is 8 nm. The particles were prepared by a research group at the Institute of Chemistry, Chinese Academy of Sciences through a so-called one-pot thermal decomposition process [17]–[19].

### III. RESULTS AND DISCUSSION

In Figs. 3 and 4, we show the one-dimensional MRI measured by applying different  $G_z$  values. Fig. 3 represents the profile of a water column sample with square cross section. With increasing the gradient value, the profile width is increased as expected. In Fig. 4, the profile from two column samples separated by 20 mm is shown. The two peaks are separated further away as the gradient is increased. The frequency difference corresponding to the two peaks increases linearly with the gradient value.

In Fig. 5, we show the two-dimensional MRI imaging of two samples. The first one is the rectangular bar shape water

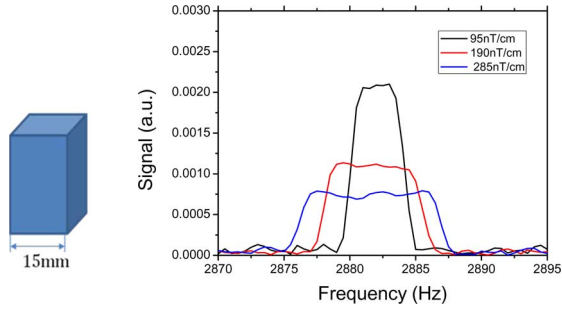


Fig. 3. NMR spectra of a square column water sample under different  $G_z$  gradients.

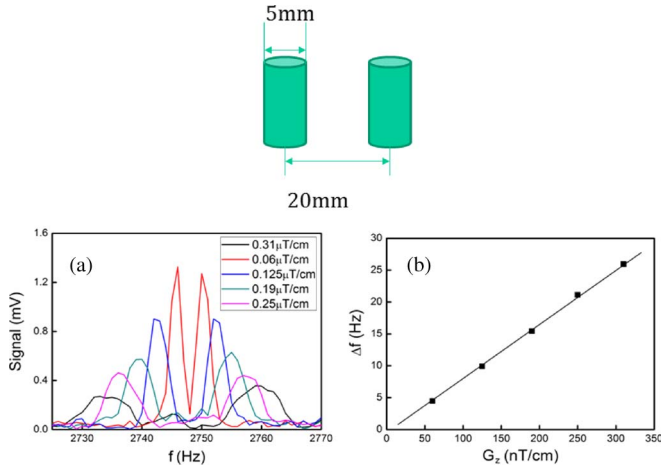


Fig. 4. (a) NMR spectra of two cylindrical columns of water separated by 20 mm under different  $G_z$  gradients. (b) Frequency difference of two peaks in Fig. 4(a) versus corresponding  $G_z$  gradients.

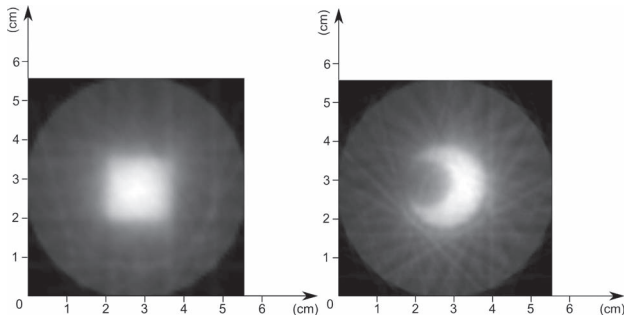


Fig. 5. 2-D MRI by back projection method. (left) 2-D image of a square column sample. (right) 2-D image of a cylinder column sample with a small solid Perspex rod inside.

column sample with a square cross section. The second one is a round water column with a piece of solid Perspex rod placed inside. Clearly, the images reflect the cross sectional shape. For the two-dimensional imaging, the sequence was similar to that used in the one-dimensional imaging, and the gradient field was applied in 12 consequence angles with  $15^\circ$  step. The field gradient was about 250 nT/cm. For each angle, the measurements were performed for several times and the data were averaged.

In MRI, images are either proton density or relaxation time weighted ( $T_1$ - or  $T_2$ -weighted). Selection depends on which type of weighting will be giving more information. In many

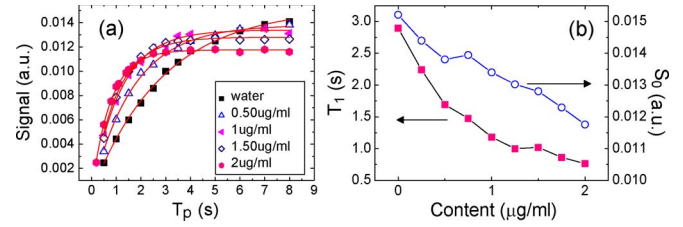


Fig. 6. (a) Intensity of NMR signal versus prepolarization time for different concentrations of  $\text{Fe}_3\text{O}_4$  MNP. (b)  $T_1$  fitted from curves in Fig. 6(a) for different concentrations of  $\text{Fe}_3\text{O}_4$  MNP.

applications of MRI, it is often to take the images based on the spin-lattice relaxation time  $T_1$  difference. Contrast agents have been developed and used to enhance MRI contrast. Usually, the contrast agents contain magnetic substances such as paramagnetic metal ions (like  $\text{Gd}^{3+}$  and  $\text{Mn}^{2+}$ ) or magnetic nano-particles (MNP).  $\text{Fe}_3\text{O}_4$  MNP is the one that commonly used. In ULF-NMR/MRI, experimental studies using different kinds of contrast agents have been carried out [4], [12], [20].

In Fig. 6, we show the results measured on a series of de-ionized water samples with addition of different amount of  $\text{Fe}_3\text{O}_4$  magnetic fluids. The MNP was prepared by a thermal decomposition method following a process similar to that described previously [17]–[19]. The average size of the  $\text{Fe}_3\text{O}_4$  MNP in the fluid is 8 nm. In the Fig. 6(a), the NMR peak height obtained from the FID data is plotted as a function of pre-polarization time  $T_p$  for different samples. In all cases, the NMR peak height is increased as  $T_p$  increased. In general, the NMR peak intensity  $s$  in the polarization process in an applied magnetic field can be described by the formula:

$$s = s_0(1 - e^{-T_p/T_1}).$$

Here  $s_0$  is the peak height when  $T_p \gg T_1$ , i.e., the value when the distribution of nuclear magnetic moment has reached the thermal equilibrium for the pre-polarization field used.  $T_1$  values can be obtained by fitting the measured data, displayed in Fig. 6(a), to the formula for each sample. The solid lines in Fig. 6(a) represent the fitting curves. In Fig. 6(b),  $T_1$  and  $s_0$  are plotted as a function of the  $\text{Fe}_3\text{O}_4$  content. The  $T_1$  value for pure water sample is about 2.8 s which is in agreement with the typical value reported. The data in Fig. 6(b) show clearly that both  $T_1$  and  $s_0$  decrease with increasing  $\text{Fe}_3\text{O}_4$  content. The magnetic moment associated with the MNP fluctuates and alters the local magnetic field in its vicinity. The interaction between the NMPs and  $^1\text{H}$  nuclei enhanced the energy dissipation process of the nuclei. Thus the spin-lattice relaxation rate is increased and  $T_1$  becomes smaller. With smaller  $T_1$  and reduced local field homogeneity, the effective spin-spin relation time  $T_2^*$  is also reduced and thus the FID with fast decay results in reduced  $s_0$ .

In Fig. 7, we show 2D MRI images of two water column samples. The one on the right contains  $\text{Fe}_3\text{O}_4$  MNP (2  $\mu\text{g}/\text{ml}$ ) and the one on the left contains pure water. When we use short  $T_p$  (0.5 s), we could see clear difference between the two. In comparison, the results measured with  $T_p = 8$  s, the difference is less significant. Therefore, an enhanced image contrast is demonstrated.

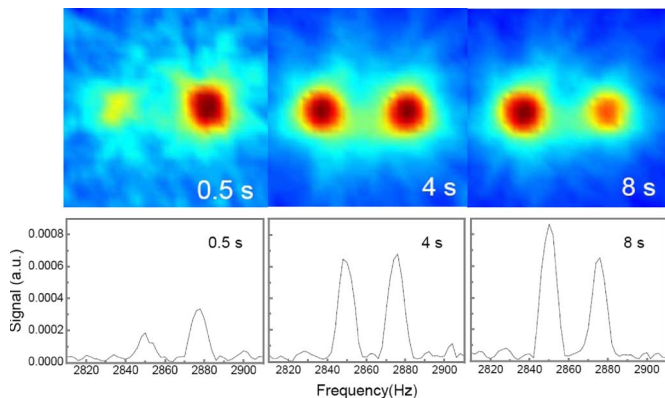


Fig. 7. Demonstration of  $T_1$ -contrast 2-D MRI (upper panel). Three images from left to right correspond to pre-polarization time of 0.5, 4, and 8 s, respectively. The sample consists of two water columns as shown in Fig. 4, with the right-hand side column added  $2 \mu\text{g/ml}$   $\text{Fe}_3\text{O}_4$  MNP. The intensity in each image is normalized to the maximum value in the image. The lower panel shows 1-D intensity plot along the line connecting the center of two columns.

#### IV. CONCLUSION

In summary, we have carried out experimental study of ULF-NMR/MRI by using a high- $T_c$  dc-SQUID sensor inside a home-made magnetically shielded room. NMR spectra of  $^1\text{H}$  of water samples were obtained in the field range  $10\text{--}110 \mu\text{T}$ . By adapting a transformer coupled detection system, the SNR of NMR peak in a single-shot measurement for 10 ml of water was increased significantly as compared with our previously used direct detection method. By applying magnetic field gradient in three directions, magnetic resonance imaging results of water samples were obtained. The results measured on water samples mixed with MNPs show decreased spin-lattice relaxation time. By varying the pre-polarization time, we could demonstrate the enhanced image contrast for samples with and without  $\text{Fe}_3\text{O}_4$  MNPs.

#### REFERENCES

- [1] Y. S. Greenberg, "Application of superconducting quantum interference devices to nuclear magnetic resonance," *Rev. Mod. Phys.*, vol. 70, no. 1, pp. 175–222, Jan. 1998.
- [2] B. Goodson, "Mobilizing magnetic resonance," *Phys. World*, vol. 19, no. 5, pp. 28–33, May 2006.
- [3] R. McDermott, A. H. Trabesinger, M. Mueck, E. L. Hahn, A. Pines, and J. Clarke, "Liquid-state NMR and scalar couplings in microtesla magnetic fields," *Science*, vol. 295, no. 5563, pp. 2247–2249, Mar. 2002.
- [4] R. McDermott, N. Kelso, S. Lee, M. Mölle, M. Mück, W. Myers, B. T. Haken, H. Seton, A. Trabesinger, A. Pines, and J. Clarke, "SQUID-detected magnetic resonance imaging in microtesla magnetic fields," *J. Low Temp. Phys.*, vol. 135, no. 5/6, pp. 793–821, Jun. 2004.
- [5] H. C. Seton, J. M. S. Hutchison, and D. M. Bussell, "A 4.2 K receiver coil and SQUID amplifier used to improve the SNR of low-field magnetic resonance images of the human arm," *Meas. Sci. Technol.*, vol. 8, no. 2, pp. 198–297, Feb. 1997.
- [6] H. C. Yang, S. H. Liao, H. E. Horng, S. L. Kuo, H. H. Chen, and S. Y. Yang, "Enhancement of nuclear magnetic resonance in microtesla magnetic field with prepolarization field detected with high- $T_c$  superconducting quantum interference device," *Appl. Phys. Lett.*, vol. 88, no. 25, pp. 252505-1–252505-3, Jun. 2006.
- [7] L. Qiu, Y. Zhang, H. Krause, A. I. Braginski, M. Burghoff, and L. Trahms, "Nuclear magnetic resonance in the earth's magnetic field using a nitrogen-cooled superconducting quantum interference device," *Appl. Phys. Lett.*, vol. 91, no. 7, pp. 072505-1–072505-3, Aug. 2007.
- [8] V. S. Zotev, A. N. Matlashov, P. L. Volegov, A. V. Urbaitis, M. A. Espy, and R. H. Kraus, Jr., "SQUID-based instrumentation for ultralow-field MRI," *Supercond. Sci. Technol.*, vol. 20, no. 11, pp. S367–S373, Nov. 2007.
- [9] V. S. Zotev, A. N. Matlashov, P. L. Volegov, I. M. Savukov, M. A. Espy, J. C. Mosher, J. J. Gomez, and R. H. Kraus, Jr., "Microtesla MRI of the human brain combined with MEG," *J. Mag. Reson.*, vol. 194, no. 1, pp. 115–120, Sep. 2008.
- [10] K. Schlenga, R. McDermott, J. Clarke, R. De Souza, A. Wong-Foy, and A. Pines, "High- $T_c$  SQUIDs for low-field NMR and MRI of room temperature samples," *IEEE Trans. Appl. Supercond.*, vol. 9, no. 2, pp. 4424–4427, Jun. 1999.
- [11] H. Dong, Y. Wang, S. Zhang, Y. Sun, and X. Xie, "Detection of proton NMR signal in the Earth's magnetic field at an urban laboratory environment without shielding," *Supercond. Sci. Technol.*, vol. 21, no. 11, p. 115 009, Nov. 2008.
- [12] S. Liao, H. Yang, H. Horng, S. Y. Yang, H. H. Chen, D. W. Hwang, and L. Hwang, "Sensitive J-coupling spectroscopy using high- $T_c$  superconducting quantum interference devices in magnetic fields as low as microteslas," *Supercond. Sci. Technol.*, vol. 22, no. 2, p. 045008, Apr. 2009.
- [13] L. Qiu, H. Krause, Y. Zhang, H. Dong, A. Braginski, and A. Offenhausser, "The effect of low frequency disturbance to SQUID based low field NMR," *IEEE Trans. Appl. Supercond.*, vol. 19, no. 3, pp. 827–830, Jun. 2009.
- [14] M. Espy, S. Baguisa, D. Dunkerley, P. Magnelind, A. Matlashov, T. Ownes, H. Sandin, I. Savukov, L. Schultz, A. Urbaitis, and P. Volegov, "Progress on detection of liquid explosives using ultra-low field MRI," *IEEE Trans. Appl. Supercond.*, vol. 21, no. 3, pp. 530–533, Jun. 2011.
- [15] A. N. Matlashov, E. Burmistrov, P. E. Magnelind, L. Schultz, A. V. Urbaitis, P. L. Volegov, J. Yoder, and M. A. Espy, "SQUID-based systems for co-registration of ultra-low field nuclear magnetic resonance images and magnetoencephalography," *Phys. C, Supercond.*, vol. 482, pp. 19–26, Nov. 2012.
- [16] Y. R. Jin, N. Wang, S. Li, Y. Tian, Y. F. Ren, Y. L. Wu, H. Deng, Y. F. Chen, J. Li, H. Y. Tian, G. H. Chen, and D. N. Zheng, "The effect of low frequency external field disturbance on the SQUID based ultra-low field NMR measurements," *IEEE Trans. Appl. Supercond.*, vol. 21, no. 3, pp. 518–521, Jun. 2011.
- [17] Z. Li, H. Chen, H. B. Bao, and M. Y. Gao, "One-pot reaction to synthesize water-soluble magnetite nanocrystals," *Chem. Mater.*, vol. 16, no. 8, pp. 1391–1393, Apr. 2004.
- [18] F. Q. Hu, L. Wei, Z. Zhou, Y. L. Ran, Z. Li, and M. Y. Gao, "Preparation of biocompatible magnetite nanocrystals for In vivo magnetic resonance detection of cancer," *Adv. Mater.*, vol. 18, no. 19, pp. 2553–2556, Oct. 2006.
- [19] F. Q. Hu, Q. J. Jia, Y. L. Li, and M. Y. Gao, "Facile synthesis of ultra-small PEGylated iron oxide nanoparticles for dual-contrast  $T_1$ - and  $T_2$ -weighted magnetic resonance imaging," *Nanotechnology*, vol. 22, no. 24, p. 245 604, Oct. 2011.
- [20] S. H. Liao, K. W. Huang, H. C. Yang, C. T. Yen, M. J. Chen, H. H. Chen, H. E. Horng, and S. Y. Yang, "Characterization of tumors using high- $T_c$  superconducting quantum interference device-detected nuclear magnetic resonance and imaging," *Appl. Phys. Lett.*, vol. 97, no. 26, pp. 263701-1–263701-3, Dec. 2010.